Volume 1 | Number 1 | Jan 2013 | Pages 1–100

Journal of
Materials Chemistry C

Materials for optical and electronic devices
www.rsc.org/materialsC

ROYAL SOCIETY
OF CHEMISTRY

ROYAL SOCIETY
OF CHEMISTRY

www.rsc.org/materialsC

A Star-shaped D-π-A Small Molecule based on a *tris*(2-methoxyphenyl)amine Core for Highly Efficient Solution-processed Organic Solar Cells

Jie Min,*[a] Yuriy N. Luponosov,[b] Alexander N. Solodukhin,[b] Nina Kausch-Busies,[c]

Sergei A. Ponomarenko,[b,d] Tayebeh Ameri,[a] Christoph J. Brabec[a,e]

[a]Institute of Materials for Electronics and Energy Technology (I-MEET), Friedrich-Alexander-University Erlangen-Nuremberg, Martensstraße 7, 91058 Erlangen, Germany
[b]Enikolopov Institute of Synthetic Polymeric Materials of the Russian Academy of Sciences, Profsoyuznaya st. 70, Moscow 117393, Russia
[c]Heraeus Precious Metals GmbH & Co. KG, Conductive Polymers Division (Clevios), Chempark Leverkusen Build. B202, D-51368 Leverkusen, Germany
[d]Chemistry Department, Moscow State University, Leninskie Gory 1-3, Moscow 119991, Russia
[e]Bavarian Center for Applied Energy Research (ZAE Bayern), Haberstraße 2a, 91058 Erlangen, Germany

E-mail: Min.Jie@ww.uni-erlangen.de (J. Min)

Abstract

A new star-shaped D-π-A small molecule, 2,2',2''-{nitrilotris[(3-methoxy-4,1-phenylene)-2,2'-bithiene-5',5-diyleth-1-yl-1-ylidene]}trimalononitrile **N(Ph(OMe)-2T-DCN-Me)$_3$**, with high efficiency potential for photovoltaic applications was synthesized. Introducing a soluble *tris*(2-methoxyphenyl)amine (TPA-MeO) core unit can significantly improve the solubility of star-shaped small molecules without negatively impacting intramolecular conjugation and intermolecular solid state arrangements. Solution-processed organic solar cells based on a blend of **N(Ph(OMe)-2T-DCN-Me)$_3$** and PC$_{70}$BM show an initially high power conversion efficiency of over 4% under simulated AM 1.5.

Introduction

The dynamic development in solution-processed small molecule organic solar cells (OSCs) has recently led to high power conversion efficiencies (PCEs) of > 8% approaching those of polymer-based devices with the most promising bulk heterojunction (BHJ) architecture.[1-3] Compared to their polymeric counterparts, structurally well-defined small molecules avoid the inherent batch-to-batch variations of physical properties and therefore provide higher reproducibility.[4-6] The current research pursuits for small molecules-based OSCs target even higher efficiencies by designing and synthesizing new organic small molecules, such as star- or X-shaped molecules,[7-10] one- or two-dimensional oligomers with D-A-D or A-D-A structures.[3,

[11-16] In particular, the most promising organic small molecule donor materials for photovoltaic applications are normally built by connecting various electron donating (donor) and electron capturing (acceptor) moieties through a π-conjugating spacer (D-π-A).[7-9, 11-16] Such a D-π-A structure can be used to lower the optical band gap to broaden molecular optical absorption and assist the formation of favorable morphologies for high photovoltaic performance.[17] A large number of D-π-A small molecules have been extensively studied and exhibited considerable molecular photovoltaic properties. For instance, Li et al. and Chen et al. synthesized two two-dimensional small molecules, D2 and DR3TBDTT with A-π-D-π-A framework which show excellent photovoltaic performance with the PCEs of up to 6.75% and 8.12%, respectively.[3, 12] Bazan and his co-workers synthesized a promising linear molecule, DTS(FBTTh$_2$)$_2$ with a high PCE up to 7%,[18] and then introduced an optical spacer (ZnO) between the aluminum cathode and the photoactive layers to further improve the PCE.[1b] More recently, using a two-dimensional conjugated small molecule (SMPV1), the best PCE of OSCs reached 8% for single junction solar cells, and 10% for double-junction tandem OSCs,[19] endowing organic small molecules with a great application potential for the generation of low cost solar cells.

However, compared to π-conjugated polymers, relatively short conjugated backbone of D-π-A linear small molecules reduces the tendency for the formation of interpenetrating networks and mixed morphologies when blended with fullerene derivatives.[20] The limited conjugation length also makes charge transport in these materials primarily intermolecular with a negligible intramolecular component, which

increases charge recombination in OSCs.[8b] In addition, the dependence of photovoltaic performance on spin-coated processing system further limits the applications of these materials in roll-to-roll processed flexible photovoltaic devices. Overcoming these obstacles requires to enhance intramolecular π-π stacking interactions, facilitate charge transport and form process-insensitive morphology in OSCs, as well as to further increase the PCE. A promising approach is to incorporate star-shaped conjugated structures into D-π-A conjugated systems.[7, 8, 20] These star-shaped molecules, which enhance intramolecular π-π interactions and extend the conjugated surface of small molecules, can effectively utilize in OSCs using doctor-bladed process.[7, 8] These results drive us to pay more attention to the high performance star-shaped small molecules for OSCs.

In recent years, star-shaped molecules have been developed as an interesting class of semiconducting materials because of their good solubility and high hole mobility.[5, 8, 21, 22] However, analyzing the performance of one- or two-dimensional small molecules for OSCs, star- or X-shaped molecules encountered a huge bottleneck due to the relatively low fill factor (FF) and modest short circuit current (J_{sc}). Nevertheless, several interesting insights were achieved for three-dimensional star-shaped molecules. Tu et al. reported a spiro-fluorene based star-shaped molecules, SF8TBT, which showed a high PCE of 4.82%, with a FF of 56%.[23] Moreover, a comparable PCE was also achieved for the triphenylamine (TPA) based molecule N(Ph-2T-DCN-Me)$_3$[8a] after optimizing the alkyl chain position and length and thus reducing the steric hindrance and torsional interactions between D/A units and

bithiophene π-bridges. However, N(Ph-2T-DCN-Me)₃ was found to be significantly less soluble at room temperature, thereby limiting the selection of printing methods for OSC processing. In addition, and due to the importance of the molecular design of the alkyl side chain position and length with respect to solubility and film morphology,[7, 8] in this contribution, we introduce a novel *tris*(2-methoxyphenyl)amine (TPA-MeO) donor unit as a core. We synthesized a new star-shaped small molecule of **N(Ph(OMe)-2T-DCN-Me)₃** with electron-withdrawing dicyanovinyl (DCN) end groups and bithiophene as the π-bridges (**Scheme 1**). Since the introduction of a methoxy side chain in **N(Ph(OMe)-2T-DCN-Me)₃** obviously does not enhance steric hindrance or cause intramolecular torsional interactions between bithiophene bridges and end groups, this strategy allows to design superior solution processability as compared to that of N(Ph-2T-DCN-Me)₃, in combination with good thermal stability and high charge carrier mobilities in blends with [6,6]-phenyl-C71-butyric acid methyl ester (PC₇₀BM). Solution-processed bulk heterojunction (BHJ) OSCs based on **N(Ph(OMe)-2T-DCN-Me)₃**:PC₇₀BM (1:2, wt%) exhibit a high PCE of 4.38% with V_{oc} of 0.88 V, J_{sc} of 9.15 mA cm^{-2}, and FF of 54.4%, under the illumination of AM1.5G, 100 mW cm^{-2}.
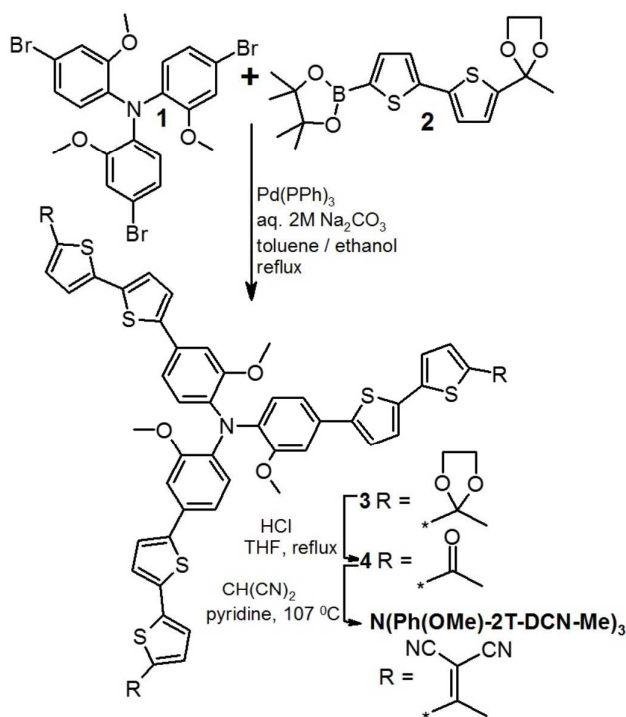
Scheme 1. Synthesis of **N(Ph(OMe)-2T-DCN-Me)₃**.

Results and discussion

Synthesis and Characterization of N(Ph(OMe)-2T-DCN-Me)₃

Preparation of this molecule was based on previously developed synthetic approach for triphenylamine-based analogues[7,8] and includes the synthesis of the star-shaped molecule with protected carbonyl groups (**3**) via Suzuki cross-coupling of **1** and **2** followed by the deprotection reaction and the final Knövenagel condensation of triketone (**4**) with malononitrile under a microwave heating (**Scheme 1**). The thermal properties were investigated by thermogravimetric analysis (TGA) and differential scanning calorimetry (DSC). **Figure S1** (see Supporting Information) shows the results of TGA of the studied compound in the air and nitrogen flow correspondingly. TGA reveals an onset decomposition

temperature (at 5% weight-loss (T_d)) in air and under inert atmosphere at approx. 402 ^{o}C (**Figure S1**), which is adequately suitable for OSC fabrication and evaluation. The first DSC trace of the novel molecule shows a melting peak at 248 °C with ΔH = 53.48 J g^{-1}, which underlines the crystalline nature of this material when processed from solution. However, subsequent cooling and second heating (**Figure S2**) show the otherwise amorphous nature of **N(Ph(OMe)-2T-DCN-Me)$_3$** with the glass transition temperature at approx. 130 ºC, which is 22 °C less as compared to its analog without methoxy groups N(Ph-2T-DCN-Me)$_3$.[8a,b] Solubility of this compound was determined in *o*-dichlorobenzene (ODCB) at room tempearture by a reproted method.[8b] Due to the solubilizing methoxy-substituents, **N(Ph(OMe)-2T-DCN-Me)$_3$** possesses good room temperature solubility (14 mg mL^{-1}) in ODCB, which is almost 5 times higher than that of N(Ph-2T-DCN-Me)$_3$ (<3 mg mL^{-1}).[8a]

Photophysical and Electrochemical Properties

Figure 1a summarizes the UV-vis absorption of **N(Ph(OMe)-2T-DCN-Me)$_3$** in ODCB solution and a thin solid film. In solution, the absorption peak at around 375 nm corresponds to the π-π^* transition of the conjugated backbone, whereas the lower energy absorption band peaking at 513 nm is ascribed to the intermolecular charge transfer (ICT) transition.[7, 8a] In comparison to their absorption in solution, the molecular absorption bands in film were red-shifted, extending the absorption edge from 604 nm in solution to 656 nm in the solid state, corresponding to an

optical band gap (E_g) of 1.89 eV. The absorption peak of the thin film (523 nm) is

bathochromically shifted by 10 nm relative to that in the solution (513 nm).

The electrochemical properties of **N(Ph(OMe)-2T-DCV-Me)₃** were investigated

using cyclic voltammetry (CVA) (**Figure 1b**). The measurements were carried out

in the 1,2-dichlorobenzene:acetonitrile (4:1) mixture of solvents using 0.1 M

Bu₄NPF₆ as a supporting electrolyte. The onset of the reduction potential (φ_{red}) is -

0.95 V vs. SCE, while the onset of the oxidation potential (φ_{ox}) is 0.90 V vs. SCE.

The lowest unoccupied molecular orbital (LUMO) and highest occupied molecular

orbital (HOMO) energy levels were correspondingly calculated to be -3.45 and -

5.30 eV, according to LUMO = - e(φ_{red} + 4.40)(eV) and HOMO = - e(φ_{ox} +

4.40)(eV).[24] In comparison to the HOMO level of N(Ph-2T-DCN-Me)₃ (-5.32

eV),[8a] **N(Ph(OMe)-2T-DCV-Me)₃** showed a higher HOMO energy level, which

should result in lower V_{oc} because the V_{oc} is usually proportional to the difference

between the LUMO leel of acceptor and the HOMO level of donor.[25]
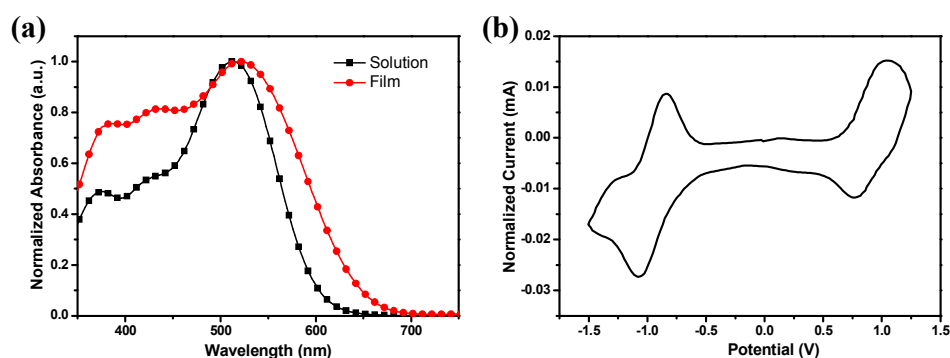
Figure 1. (a) Absorption spectra of **N(Ph(OMe)-2T-DCN-Me)₃** in ODCB and thin

film. (b) Cyclic voltammogram (1-st peaks, potentials vs. SCE) of the molecule

measured in the ODCB: acetonitrile (4:1) mixture of solvents using 0.1 M

Bu$_4$NPF$_6$ as a supporting electrolyte.

Photovoltaic properties

The photovoltaic properties of **N(Ph(OMe)-2T-DCN-Me)$_3$** were preliminarily investigated by fabricating solution-processed BHJ devices in the conventional structure glass/ITO/PEDOT:PSS/**N(Ph(OMe)-2T-DCN-Me)$_3$**:PC$_{70}$BM/various cathodes. The detailed device fabrication process is described in Experimental Section. To optimize the device condition, devices with different donor-acceptor weight ratios were examined, as shown in **Figure S3** and **Table S1**. All the devices yield relatively high V_{oc} (0.88-0.90 V) which are consistent with the deeper low-lying HOMO and are relatively insensitive to the donor:acceptor (D:A) blend ratio. Even though the weight ratios of active layer had a huge difference from 1:1 to 1:3, **N(Ph(OMe)$_3$-2T-DCV-Me)$_3$**:PC$_{70}$BM based devices exhibited stable PCE values over 3%, as shown in **Table S1**. It was presented that the OSC with the D:A weight ratio of 1:2 showed the best PCE of 3.92% with a V_{oc} of 0.88 V, a J_{sc} of of 8.45 mA cm^{-2} and a FF of 52.7%, under the illumination of AM 1.5G at 100 mW cm^{-2}. Compared to the performance of N(Ph-2T-DCN-Me)$_3$:PC$_{70}$BM based device,[8a] the device using the **N(Ph(OMe)$_3$-2T-DCV-Me)$_3$**:PC$_{70}$BM blend showed lower V_{oc} (0.98 V vs. 0.88 V), which was consistent with the higher HOMO level due to electron donating methoxy substituents. However, **N(Ph(OMe)$_3$-2T-DCV-Me)$_3$** is more suitable for solution process electronic devices. Since the photovoltaic performance frequently depends on the choice of the cathode,[1, 8c] we further studied the impact of

various cathode materials including Al, Ca/Al and ZnO/Al, on the photovoltaic performance. **Figure 2** shows the current density-voltage (J–V) curves of the OSC based on **N(Ph(OMe)-2T-DCN-Me)$_3$**:PC$_{70}$BM (1:2, wt%) with various cathodes as well as the external quantum efficiency (EQE) plots. Compared to the devices with Ca/Al and ZnO/Al cathodes, the device with Al cathode showed a low V_{oc} (0.88 V vs. 0.85 V), which is consistent with the unsuitable contact formation between the active layer and Al cathode. In contrast, the Ca/Al device exhibits higher photovoltaic parameters due to enhanced charge extraction. The device was further improved by inserting a thin ZnO layer (25 nm) between the active layer and Al cathode. Compared to the performance of the Al-only device, the PCE of device with ZnO interfacial layer increases from 2.82% to 4.38%, mainly due a higher J_{sc} of 9.15 mA cm^{-2} and a better FF of 54.4%, as shown in **Figure 2** and **Table 1**. The EQE curves of the devices symbiotically covered a broad wavelength range of 300-670 nm, and suggests that at the analysed film thickness both, **N(Ph(OMe)-2T-DCN-Me)$_3$** and PC$_{70}$BM contribute to the photo-current. In addition, the EQE curves are well consistent with the J_{sc} values measured under simulated AM 1.5.
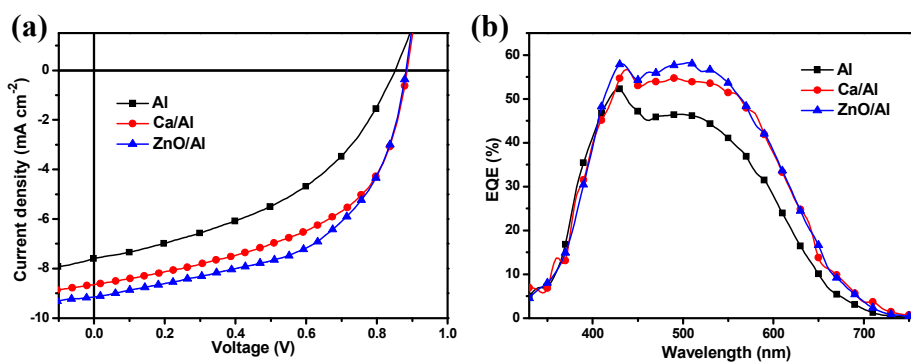
Figure 2. (a) The J–V curves of the **N(Ph(OMe)-2T-DCN-Me)$_3$**:PC$_{70}$BM OSCs with

various cathodes under the illumination of AM 1.5G at 100 mW cm^{-2}, (b) the EQE

curves of the devices.

Table 1. The photovoltaic performance of the OSCs based on N(Ph(OMe)-2T-DCV-

Me)$_3$:PC$_{70}$BM blends, under the illumination of AM 1.5G at 100 mW cm^{-2}

Cathodes	V_{oc} [V]	J_{sc} [mA cm^{-2}]	FF [%]	PCE$_{max}$ (PCE$_{ave}$[a])[%]
Al	0.85	7.60	43.6	2.82 (2.73)
Ca/Al	0.88	8.45	52.7	3.92 (3.80)
ZnO/Al	0.88	9.15	54.4	4.38 (4.25)

[a]The average PCE is obtained from six cells.

Film morphology and charge transport

Nanoscale phase separtion in the morphology of the active layer is required for

high performance OSCs, which enables a large interfacial area for exciton

dissociation and a continuous percolating path for hole and electron transport to

the corresponding electrodes.[26] Here, the atomic force microscopy (AFM) images

of the active layer were examined with and without a top ZnO layer, as shown in

Figure 3. The AFM phase image of the blend film of N(Ph(OMe)-2T-DCN-

Me)$_3$:PC$_{70}$BM (1:2, wt%), exhibited a smooth surface (root mean square (RMS)

roughness of 0.35 nm) with a good interconnected regions and domains, which is

beneficial to exciton dissociation and charge carrier transport.[26] **Figure 3b** shows

that the ZnO nanoparticles were evenly deposited on the surface of the active layer.

Deposition of ZnO nanoparticles on the active laeyr under the experimental conditions described here also resulted in increased roughness from 0.35 nm to 5.76 nm.

The hole and electron mobility of **N(Ph(OMe)₃-2T-DCV-Me)₃** were determined via the space charge limited current (SCLC) methode with the deivce structure glass/ITO/PEDOT:PSS/active layer/MoO₃/Ag (100 nm) and ITO/aluminum doped ZnO (AZO)/active layer/Ca/Ag, respectively. We calibrated the hole and electron mobility by fitting the current-voltage curves over six diodes,[7] as shown in **Figure 4**. The hole and electron mobility obtained for the **N(Ph(OMe)₃-2T-DCV-Me)₃**:PC₇₀BM (1:2, wt%) blend films are 5.19×10^{-5} and 1.25×10^{-3} cm² V^{-1}s^{-1}, respectively.
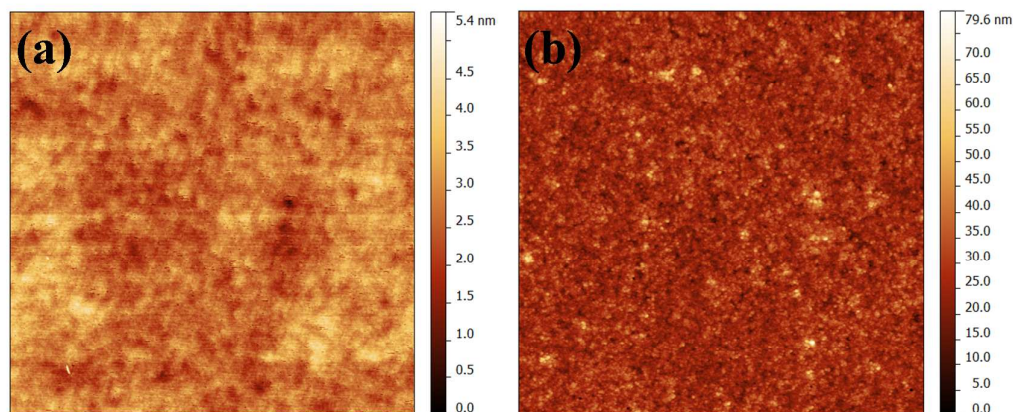
Figure 3. Tapping mode AFM surface scans (5×5 μm²) of the **N(Ph(OMe)-2T-DCN-Me)₃**:PC₇₀BM (1:2, wt%) blends (a) without and (b) with ZnO layer. The film surfaces show the root-mean-square (RMS) roughness of 0.35 nm for (a) and 5.76 nm for (b).
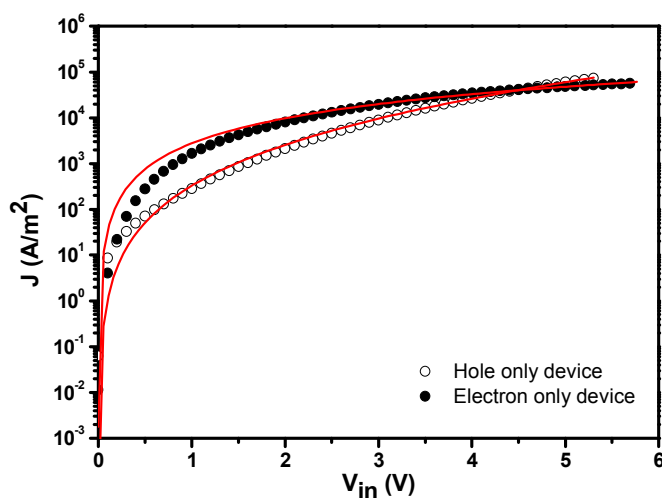
Figure 4. Hole only mobility and electron only mobility of **N(Ph(OMe)-2T-DCN-Me)$_3$**:PC$_{70}$BM (1:2, wt%) blended films.

Conclusions

In conclusion, a new star-shaped small molecule, **N(Ph(OMe)-2T-DCN-Me)$_3$**, with D-π-A framework was synthesized. It has excellent solution processing conditions due to the more soluble TPA-MeO core unit. The BHJ OSCs based on **N(Ph(OMe)-2T-DCN-Me)$_3$**:PC$_{70}$BM (1:2, wt%) as active layer and with ZnO/Al as cathode show an initially high PCE of 4.38% without any special treatment needed. This preliminary work demonstrates that the TPA-MeO donor unit offers a good strategy to improve the solubility of star-shaped small molecule donor materials without negatively impacting intramolecular conjugation and intermolecular solid state arrangements. In addition, the optimized performance of device using ZnO layer suggests that this device structure is especially useful in roll-to-roll processing flexible and large-area electronics.

Experimental Section

General

GPC analysis was performed by means of a Shimadzu LC10A^{VP} series chromatograph (Japan) equipped with an RID-10A^{VP} refractometer and SPD-M10A^{VP} diode matrix as detectors and a Phenomenex column (USA) with a size of 7.8×300 mm^2 filled with the Phenogel sorbent with a pour size of 500 Å; THF was used as the eluent. For thin layer chromatography, "Sorbfil" (Russia) plates were used. In the case of column chromatography, silica gel 60 ("Merck") was taken.

^{1}H NMR spectra were recorded at a "Bruker WP-250 SY "spectrometer, working at a frequency of 250.13 MHz and utilising CDCl$_3$ signal (7.25 ppm) as the internal standard. ^{13}C NMR spectra were registered on Bruker DRX500 a frequency of 125 MHz. In the case of ^{1}H NMR spectroscopy, the compounds to be analysed were taken in the form of 1% solutions in CDCl$_3$. In the case of ^{13}C NMR spectroscopy, the compounds to be analysed were taken in the form of 5% solutions in CDCl$_3$. The spectra were then processed on the computer using the ACD Labs software.

Mass-spectra (MALDI) were registered on the Autoflex II Bruker (resolution FWHM 18000), equipped with nitrogen laser (work wavelength 337 nm and time-of-flight mass-detector working in reflections mode. The accelerating voltage was 20 kV. Samples were applied to a polished stainless steel substrate. Spectrum was recorded in the positive ion mode. The resulting spectrum was the sum of 300 spectra obtained at different points of sample. 2, 5-dihydroxybenzoic acid (DHB) (Acros, 99%) and α-

cyano-4-hydroxycinnamic acid (HCCA) (Acros, 99%) were used as matrices.

Elemental analysis of C, H, N elements was carried out using CHN automatic analyzer CE 1106 (Italy). The settling titration using $BaCl_2$ was applied to analyze sulphur. Experimental error is 0.30-0.50%.

The Knövenagel condensation was carried out in the microwave "Discovery", (CEM corporation, USA), using a standard method with the open vessel option, 50 watts.

Thermogravimetric analysis was carried out in dynamic mode in $30 \div 900°C$ interval using *Mettler Toledo* TG50 system equipped with M3 microbalance allowing measuring the weight of samples in $0 \div 150$ mg range with $1 \square g$ precision. Heating/cooling rate was chosen to be $10°C$ min^{-1}. The compound was studied twice: in air and in nitrogen flow of 200 mL min^{-1}.

DSC scans were obtained with *Mettler Toledo* DSC30 system with $20°C$ min^{-1} heating/cooling rate in temperature range of $+20 \div 250°C$ for the compound. Nitrogen flow of 50 mL min^{-1} was used.

Absorption profiles were recorded with a Perkin Elmer Lambda-35 absorption spectrometer from 350 to 1100. Electrochemical properties were studied by cyclic voltammetry (CVA). The measurements were carried out in the 1, 2-dichlorobenzene: acetonitrile (4:1) mixture of solvents using 0.1 M Bu_4NPF_6 as supporting electrolyte. The glassy carbon electrode was used as a work electrode. Potentials were measured relative to a saturated calomel electrode.

Materials

Tetrakis(triphenylphosphine)palladium(0)Pd(PPh$_3$)$_4$, malononitrile were obtained

from Sigma–Aldrich Co. and used without further purification. Pyridine were dried and purified according to the known techniques and then used as solvents. *Tris*(4-bromo-2-methoxyphenyl)amine was obtained as described in Ref. [27]. The 2-[5'-(2-methyl-1,3-dioxolan-2-yl)-2,2'-bithien-5-yl]-4,4,5,5-tetramethyl-1,3,2 -dioxaborolane (**2**) was obtained as described previously.[8a]

Synthesis

Tris{2-methoxy-4-[5'-(2-methyl-1,3-dioxolan-2-yl)-2,2'-bithien-5-yl]phenyl}amine (**3**). In an inert atmosphere, degassed solutions of tris(4-bromo-2-methoxy-phenyl)amine (**1**) (2.24 g, 3.9 mmol) and 2-[5'-(2-methyl-1,3-dioxolan-2-yl)- 2,2'-bithien-5-yl]-4,4,5,5-tetramethyl-1,3,2-dioxaborolane (**2**) (5.33 g, 14.1 mmol) in toluene/ethanol mixture (70/7 mL) and 2M solution of aq. Na_2CO_3 (21.1 mL) were added to $Pd(PPh_3)_4$ (489 mg, 0.4 mmol). The reaction mixture was stirred under reflux for 10 h, and then it was cooled to room temperature and poured into 150 mL of water and 150 mL of toluene. The organic phase was separated, washed with water, dried over sodium sulfate and filtered. The solvent was evaporated in vacuum and the residue was dried at 1 Torr. The product was purified by column chromatography on silica gel (eluent toluene) to give pure compound 4 (3.6 g, 84%) as yellow solid. ^{1}H NMR (250 MHz, $CDCl_3$): δ [ppm] 1.79 (s, 9H), 3.66 (s, 9H), 3.92–4.15 (overlapping peaks, 12H), 6.83 (d, 3H, J = 8.7 Hz), 6.93 (d, 3H, J = 3.7 Hz), 7.01 (d, 3H, J = 3.7 Hz), 7.04-7.12 (overlapping peaks, 9H), 7.15 (d, 3H, J = 3.7 Hz). ^{13}C NMR (125 MHz, $CDCl_3$): δ [ppm] 27.51, 55.96, 65.05, 107.11, 109.82, 118.17, 123.04, 123.1, 124.51, 124.76, 124.91, 130.1, 135.91, 136.68, 137.19, 143.43, 146.14, 153.14. Calcd (%) for $C_{57}H_{51}NO_9S_6$: C, 63.02; H, 4.73; N, 1.29; S, 17.71. Found: C, 62.88; H, 4.75; N, 1.22; S, 17.47. MALDI-MS: found m/z 1084.68; calculated for $[M]^+$ 1085.18.

1,1',1''-{nitrilotris[(3-methoxy-4,1-phenylene)-2,2'-bithiene-5',5-diyl]}triethanone (4). 1M HCl (5.52 mL) was added to a solution of compound **3** (3.00 g, 2.8 mmol) in

THF (20 mL) and then the reaction mixture was stirred for 3 hours at reflux at boiling temperature. During the reaction the product was gradually formed as orange precipitate. After completion of the reaction the organic phase was separated using diethyl ether, washed with water and filtered off to give pure compound **4** (2.27 g, 86%) as orange crystals. ^{1}H NMR (250 MHz, CDCl$_3$): δ [ppm] 2.54 (s, 9H), 3.67 (s, 9H), 6.85 (d, 3H, J = 9.1 Hz), 7.02-7.14 (overlapping peaks, 6H), 7.16 (d, 3H, J = 4.3 Hz), 7.20 (d, 3H, J = 4.3 Hz), 7.27 (d, 3H, J = 3.7 Hz), 7.58 (d, 3H, J = 4.3 Hz). ^{13}C NMR (125 MHz, CDCl$_3$): δ [ppm] 26.65, 56.13, 110.17, 118.59, 123.59, 123.88, 124.99, 126.75, 129.91, 133.55, 134.88, 137.12, 142.28, 145.81, 146.03, 153.33, 190.38. Calcd (%) for C$_{51}$H$_{39}$NO$_6$S$_6$: C, 64.19; H, 4.12; N, 1.47; S, 20.16. Found: C, 64.27; H, 4.26; N, 1.46; S, 20.21. MALDI-MS: found m/z 952.66; calculated for [M]$^+$ 953.11.

2,2',2"-{nitrilotris[(3-methoxy-4,1-phenylene)-2,2'-bithiene-5',5-diyleth-1-yl-1-ylidene]}trimalononitrile (N(Ph(OMe)-2T-DCN-Me)$_3$). Compound **4** (2.42 g, 2.5 mmol), malononitrile (1.17 g, 17.8 mmol) and dry pyridine (50 mL) were placed in a reaction vessel and stirred under argon atmosphere for 8 hours at 107 ℃ using the microwave heating. After completeness of the reaction the pyridine was evaporated in vacuum and the residue was dried at 1 Torr. This crude product was purified by column chromatography on silica gel (eluent dichloromethane). Further purification included precipitation of the product from its THF solution with toluene and hexane to give pure product as a black solid (1.82 g, 67%). ^{1}H NMR (250 MHz, CDCl$_3$): δ [ppm] 2.67 (9H, s), 3.68 (9H, s), 6.87 (d, 3H, J = 7.9 Hz), 7.07-7.15 (overlapping

peaks, 6H), 7.26 (d, 3H, J = 4.3 Hz), 7.35 (d, 3H, J = 4.3 Hz), 7.94 (d, 3H, J = 4.3 Hz). ^{13}C NMR (125 MHz, CDCl$_3$): δ [ppm] 23.18, 56.15, 110.17, 114.14, 114.69, 118.68, 123.92, 124.66, 125.06, 127.82, 129.69, 133.68, 135.56, 135.78, 137.28, 147.17, 153.37, 161.12. Calcd (%) for C$_{60}$H$_{39}$N$_7$O$_3$S$_6$: C, 65.61; H, 3.58; N, 8.93; S, 17.51. Found: C, 65.82; H, 3.72; N, 8.71; S, 17.29. MALDI-MS: found m/z 1096.65; calculated for [M]$^+$ 1097.14.

Device Fabrication

Photovoltaic devices were fabricated by doctor-blading on indium-tin oxide (ITO)-covered glass substrates (from Osram). These substrates were cleaned in toluene, water, acetone, and isopropyl alcohol. After drying, the substrates were bladed with 40 nm PEDOT:PSS (HC Starck, PEDOT PH-4083). Photovoltaic layers, consisting of **N(Ph(OMe)-2T-DCN-Me)$_3$** and PC$_{70}$BM in different weight ratios, were dissolved at the concentration of 1% (10 mg mL^{-1}) in dichlorobenzene (ODCB) and bladed on top of the PEDOT:PSS layer. Finally, a calcium/aluminum top electrode of 15/80 nm thickness or an aluminum top electrode of 100 nm thickness was evaporated on top of photoactive layer. In addition, the ZnO layer (25 nm) (provided by NanoGrade, Lot #5039), was bladed on top of the photoactive layer. After that, an aluminum top electrode of 100 nm thickness was evaporated. The typical active area of the investigated devices was 10.4 mm^2. The current-voltage characteristics of the solar cells were measured under AM 1.5G irradiation on an OrielSol 1A Solar simulator (100 mW cm^{-2}). The external quantum efficiencies (EQE) was detected with Cary 500

Scan UV-Vis-NIR spectrophotometer under monochromatic illumination, which was calibrated with a mono-crystalline silicon diode. The characterization of the current density-voltage (*J–V*) curve was done in an inert nitrogen atmosphere and the EQEs of the devices without encapsulation were measured in air.

AFM measurements were performed with a Nanosurf Easy Scan 2 in contact mode. Single carrier devices were fabricated and the dark current-voltage characteristics measured and analyzed in the space charge limited (SCL) regime following the reference [7]. The structure of hole only devices was Glass/ITO/PEDOT:PSS/active layer/MoO$_3$/Ag (100 nm). For the electron only devices, the structure was Glass/ITO/AZO/active layer/Ca (15 nm)/Ag (100 nm), where both Ca and Ag were evaporated. The reported mobility data are average values over the six devices of each sample at a given film composition.

Electronic supplementary information (ESI) available: TGA and DSC plots, *J-V* curves of OSCs with various D:A ratios, and ^{1}H and ^{13}C NMR spectra of monomers.

which is funded by the German Research Foundation (DFG) within the framework of its ''Excellence Initiative''. This work has been partially funded by the Sonderforschungsbereich 953 "Synthetic Carbon Allotropes", the China Scholarship Council (CSC) and the Russian Scientific Foundation (RNF).

References

[1] V. Gupta, A. K. K. Kyaw, D. H. Wang, S. Chand, G. C. Bazan, A. J. Heeger, *Sci Rep*. 2013, **3**, 1965. (b) A. K. K. Kyaw, D. H. Wang, D. Wynands, J. Zhang, T-Q. Nguyen, G. C. Bazan, A. J. Heeger, *Nano Lett*., 2013, **13**, 3796.

[2] A. K. K. Kyaw, D. H. Wang, V. Gupta, W. L. Leong, L. Ke, G. C. Bazan, A. J. Heeger, *ACS Nano*, 2013, **7**, 4569.

[3] J. Y. Zhou, Y. Zou, X. J. Wan, G. K. Long, Q. Zhang, W. Ni, Y. S. Liu, Z. Li, G. R. He, C. X. Li, B. Kan, M. M. Li, Y. S. Chen, *J. Am. Chem. Soc*., 2013, **135**, 8484.

[4] B. Walker, C. Kim and T. Q. Nguyen, *Chem. Mater*. 2010, **23**, 470.

[5] J. Roncali, *Acc. Chem. Res*. 2009, **42**, 1719.

[6] Y. Z. Lin, Y. F. Li, X. W. Zhan, *Chem. Soc. Rev*., 2012, **41**, 4245.

[7] J. Min, Y. N. Luponosov, T. Ameri, A. Elschner, S. M. Peregudova, D. Baran, T. Heumüller, N. Li, F. Machui, S. Ponomarenko, C. J. Brabec, *Org. Electron*. 2013, **14**, 219.

[8] (a) J. Min, Y. N. Luponosov, A. Gerl, M. S. Polinskaya, S. M. Peregudova, P. V. Dmitryakov, A. V. Bakirov, M. A. Shcherbina, S. N. Chvalun, S. Grigorian, N. K. Busies, S. A. Ponomarenko, T. Ameri, C. J. Brabec, *Adv. Energy Mater*., 2014, **4**,

1301234. (b) J. Min, Y. N. Luponosov, D. Baran, S. N. Chvalun, M. A. Shcherbina, A. V. Bakirov, P. V. Dmitryakov, S.M. Peregudova, N. Kausch-Busies, S. A. Ponomarenko, T. Ameri, C. J. Brabec, *J. Mater. Chem. A*, 2014, accepted. (c) J. Min, Y. N. Luponosov, Z-G. Zhang, S. A. Ponomarenko, T. Ameri, Y. F. Li, C. J. Brabec, *Adv. Energy Mater*., 2014, accepted.

[9] H. X. Shang, H. J. Fan, Y. Liu, W. P. Hu, Y. F. Li, X. W. Zhan, *Adv. Mater*. 2011, **23**, 1554.

[10] C. Q. Ma, M. Fonrodona, M. C. Schikora, M. M. Wienk, R. A. J. Janssen, P. Bauerle, *Adv. Funct. Mater*. 2008, **18**, 3323.

[11] C. H. Cui, J. Min, C. L. Ho, T. Ameri, P. Yang, J. Z. Zhao, C. J. Brabec, W. Y. Wong, *Chem. Commun*., 2013, **49**, 4409.

[12] S. L. Shen, P. Jiang, C. He, J. Zhang, P. Shen, Y. Zhang, Y. P. Yi, Z. J. Zhang, Z. B. Li, Y. F. Li, *Chem. Mater*., 2013, **25**, 2274.

[13] Y. Z. Lin, L. C. Ma, Y. F. Li, Y. Q. Liu, D. B. Zhu, X. W. Zhan, *Adv. Energy Mater*. 2013, **3**, 1166.

[14] Y. M. Sun, G. C. Welch, W. L. Leong, C. J. Takacs, G. C. Bazan, A. J. Heeger, *Nat. Mater*, 2012, **11**, 44.

[15] Y. S. Liu, Y. Yang, C. C. Chen, Q. Chen, L. T. Dou, Z. R. Hong, G. Li, Y. Yang, *Adv. Mater*. 2013, **25**, 4657.

[16] J. Y. Zhou, X. J. Wan, Y. S. Liu, Y. Zou, Z. Li, G. R. He, G. K. Long, W. Ni, C. X. Li, X. C. Su, Y. S. Chen, *J. Am. Chem. Soc*., 2012, **134**, 16345.

[17] W. W. Li, M. Kelchtermans, M. M. Wienk, R. A. J. Janssen, *J. Mater. Chem. A*, 2013, **1**, 15150.

[18] T. S. van der Poll, J. A. Love, T. Q. Nguyen, G. C. Bazan, *Adv. Mater*. 2012, **24**, 3646.

[19] Y. S. Liu, C.-C Chen, Z. R. Hong, J. Gao, Y. (Michael) Yang, H. P. Zhou, L. T. Dou, G. Li, Y. Yang, *Sci Rep*. 2013, **3**, 3356.

[20] D. Demeter, V. Jeux, P. Leriche, P. Blanchard, Y. Olivier, J. Cornil, R. Po, J. Roncali, *Adv. Funct. Mater*. 2013, **23**, 4854.

[21] E. Ripaud, T. Rousseau, P. Leriche, J. Roncali, *Adv. Energy Mater*. 2011, **1**, 540.

[22] Z. G. Zhang, S. Y. Zhang, J. Min, C. H. Chui, J. Zhang, M. J. Zhang, Y. F. Li, *Macromolecules* 2012, **45**, 113.

[23] S. Y. Ma, Y. Y. Fu, D. B. Ni, J. Mao, Z. Y. Xie, G. L. Tu, *Chem. Commun*., 2012, **48**, 11847.

[24] S. A. Ponomarenko, N. N. Rasulova, Y. N. Luponosov, N. M. Surin, M. I. Buzin, I. Leshchiner, S. M. Peregudova, A. M. Muzfarov, *Macromolecules*, 2012, **45**, 2014.

[25] J. Min, Z. G. Zhang, M. J. Zhang, Y. F. Li, *Polym. Chem*., 2013, **4**, 1467.

[26] C. J. Brabec, A. Cravino, D. Meissner, N. S. Sariciftci, T. Fromherz, M. T. Rispens, L. Sanchez, J. C. Hummelen, *Adv. Funct. Mater*. 2001, **11**, 374.

[27] R. Alvarez, G. H. Mehl, *Tetrahedron Lett*. 2005, **46**, 67.